Chapter 2

Aerodynamics of Flapping Flight

Flying animals flap their wings to generate lift and thrust as well as to perform remarkable maneuvers with rapid accelerations and decelerations. Insects, bats and birds provide illuminating examples of unsteady aerodynamics. In this chapter we present the various issues related to the aerodynamics of flapping flight. We first present flapping flight in nature. We next review both analytical and computational models and some experimental observations. Then, we present a review of nonstationary airfoil aerodynamics including dynamic stall, vortex shedding and thrust generation; followed by a presentation of flapping wing flight in terms of Reynolds number, Strouhal number and reduced frequency. Finally, we close this chapter with a discussion of flapping wings performance parameters and flapping wings kinematics.

2.1 Flight in Nature

The fundamentals of bird flight are similar to those of aircrafts. As the wings move through the air, they are held at a slight angle, which deflects the air gently downward. This causes air pressure to build up beneath the wings, while the pressure above the wings is reduced. The difference in pressure produces lift, a force that acts roughly perpendicular to the wing surface and keeps the bird or airplane from falling. Generally, bird flight can be divided into two modes of functioning, *i.e.*, unpowered flight (gliding and soaring flight) and powered flight (flapping and hovering flight).

When a bird is gliding, the wings are held out to the side of the body and do not flap. Lift force is produced by the action of air flow on the wings. The lift force occurs because the air has a lower pressure just above the wings and higher pressure below. But there is also air resistance or drag on the body and wings of the bird. This force would eventually cause the bird to slow down, up to the point where it would not have enough speed to fly. To make up for this, the bird can lean forward a little and go into a shallow dive. In that way, the lift force produced by the wings is angled forward slightly helping the bird to speed up. Really what the bird is doing here is giving up some height in exchange for increased speed (or putting it in another way, it is converting its gravitational potential energy into kinetic energy).

An alternative method to gliding used by many biological flyers to produce lift and thrust, is flapping wing flight. Flapping flight is a far more complicated process than gliding. During flapping flight, the bird's wings systematically change shape. Flapping involves up and down movement of the wings. During the downstroke (or power stroke), the wings move downward and forward. During the upstroke (or recovery stroke), the wings move upward and drawn in toward the body

to reduce drag. During flapping flight, the wings also changes their angle of attack depending on the stroke. Flapping flight is basically rowing in the air with the added complication that lift needs to be generated as well.

2.1.1 Unpowered Flight: Gliding and Soaring

Flying animals usually flap their wings to generate both lift and thrust. But if they stop flapping and keep their wings stretched out, their wings actively produce only lift, nor thrust. Thrust can be produced by gravity force while the animal is descending. When this happens, we call them gliders. Many gliding birds (and soaring birds as well) appear to hang in the air effortlessly, gaining height with barely a twitch of a wing. These are birds like vultures, albatrosses, pelicans and storks with a high lift-to-drag ratio. Essentially, this means that their wings generate a lot of lift without producing much drag. Large birds have evolved to be gliders partly because gliding becomes easier the larger your wings are and obviously small birds can not have large wings. In addition to birds, gliders can also be found among bats, fish, amphibians, reptiles, and mammals [167].

Figure 2.1: *A bird while gliding. Notice the separation between the wingtip feathers; these natural slots, help to reduce the induced drag while gliding.*

To maintain level flight, a flying animal must produce both lift and thrust to balance the gravity force in the vertical direction and drag in the horizontal direction respectively. Because gliding occurs with no active thrust production, an animal always resorts to the gravity force to overcome the drag. In gliding, the animal tilts its direction of motion slightly downward relative to the air that it moves through. When the animal tilts downward, the resulting angle between the motion direction and the air becomes the gliding angle. The gliding angle directly controls the lift-to-drag ratio. The higher this ratio, the shallower the glide becomes. The lift-to-drag ratio increases with the Reynolds number, a parameter proportional to animal size and flight speed. Large flying animals fly at high Reynolds numbers and have a large lift-to-drag ratio. For example, a wandering albatross, with a wing span of over 3 meters, has a reported lift-to-drag ratio of 19, whereas the fruit fly, which has a span of 6 millimeters, has a lift-to-drag ratio of 1.8

[3, 200]. If the animal has a low lift-to-drag ratio, it must glide (if it can) with a considerably large glide angle. For example, the North American flying squirrel has a glide angle of about 18 to 26 degrees with a lift-to-drag ratio of 2 to 3 [3, 167].

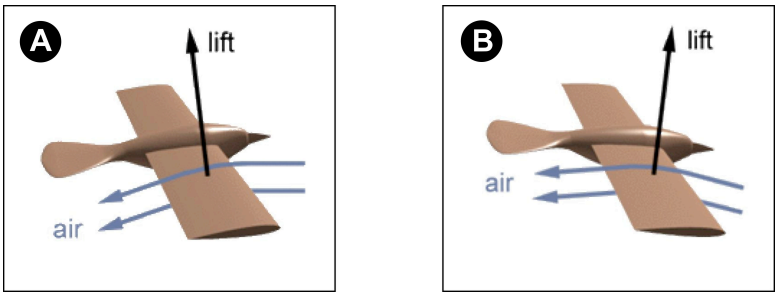

Figure 2.2: *In gliding flight, a bird's wing deflect air downward, causing a lift force that holds the bird up in the air (see figure A). By tilting forward and going into a slight dive (figure B), the bird can maintain forward speed.*

Gliding flight always results in a bird moving downward through the air. In order to maintain or gain height, birds resort to soaring (see figure 2.3). Soaring flight is a special kind of glide, in which the bird flies into a rising air current. Because the air is rising, the bird can maintain its height relative to the ground without the need of flapping its wings. Instead of using gravity, soaring uses energy in the atmosphere, such as rising air current.

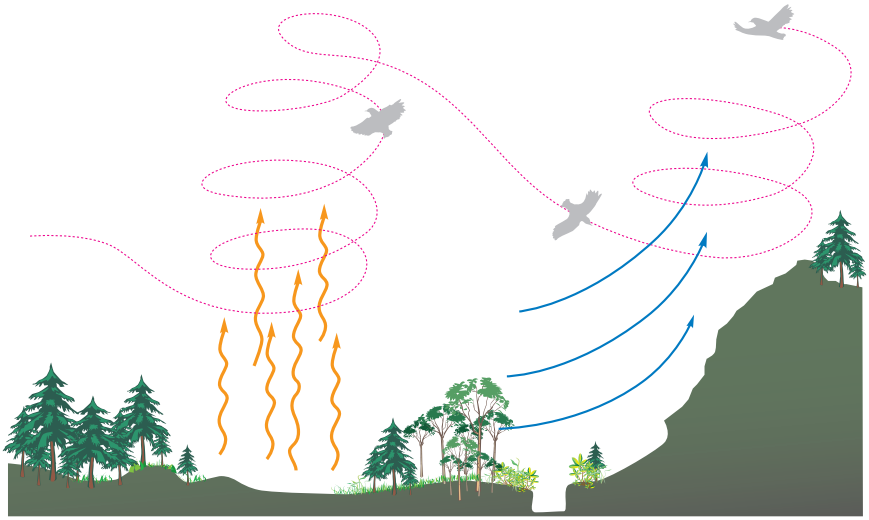

Figure 2.3: *In soaring flight, birds use both the updraft thermals and orographic lifting to maintain or gain altitude and save energy.*

2.1.2 Powered Flight: Flapping

Flapping flight is more complicated than flight with fixed wings because of the structural movement and the resulting unsteady fluid dynamics. Conventional airplanes with fixed wings are, in comparison, very simple. The forward motion relative to the air causes the wings to produce lift. However, in flapping flight the wings not only move forward relative to the air, they also flap up and down, bend, twist and sweep.

Figure 2.4: *A Mallard in powered flight (flapping flight).*

When a bird flaps, as opposed to gliding, its wings continue to develop lift as before, but they also create an additional forward and upward force, thrust, to counteract its weight and drag. Flapping involves two stages: the downstroke or power stroke, which provides the majority of the thrust, and the upstroke or recovery stroke, which can also (depending on the bird's wings) provide some upward force. At each upstroke the wing is slightly folded inwards to reduce upward resistance. Birds change the angle of attack between the upstroke and the downstroke of their wings. During the downstroke the angle of attack is increased, and is decreased during the upstroke.

When the wings move up and down, they are also moving forward through the air along with the rest of the bird. Close to the body, there is very little up and down movement. Farther out toward the wingtips, there is much more vertical motion. As the bird is flapping along, it needs to make sure it has the correct angle of attack all along its wingspan. Since the outer part of the wing moves up and down more steeply than the inner part, the wing has to twist (and bird's wings are very flexible), so that each part of the wing can maintain just the right angle of attack. As the wing twists, and as the outer part of the wing moves downward, the lift force in the outer part of the wing is angled forward. This is what would happen if the whole bird went into a steep dive. However, only the wing is moving downward, not the whole bird. Therefore the bird can generate a large amount of forward propulsive force without any loss of altitude. During this stroke, the air is not only deflected downward, but also to the rear. The air is forced backward just as it would be by a propeller.

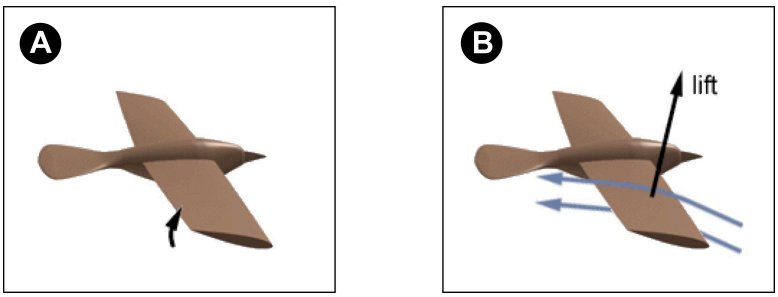

Figure 2.5: *In A, the wings twist as shown to maintain the correct angle of attack for the downstroke. In B, the bird's wings produce lift and thrust during the downstroke.*

During the upstroke, the outer part of the wing points straight along its line of travel so it can pass through the air with the least possible resistance. In other words, the angle of attack is reduced to zero. The bird partially folds its wings, which reduces the wingspan and eliminates the draggy outer part of the wing (this is not strictly necessary though, and most insects lack this capability). Also, the primaries (wingtip feathers) separate, these natural slots, allow passage of air through them, reducing in this way the skin friction.

The inner part of the wing is different. There is little up-and-down movement there, so that part of the wing continues to provide lift and functions more or less as it would when gliding. Because only the inner part of the wing produces lift in the upstroke, the upstroke as a whole offers less lift than the downstroke. As a result, the bird's body will bob up and down slightly during flight.

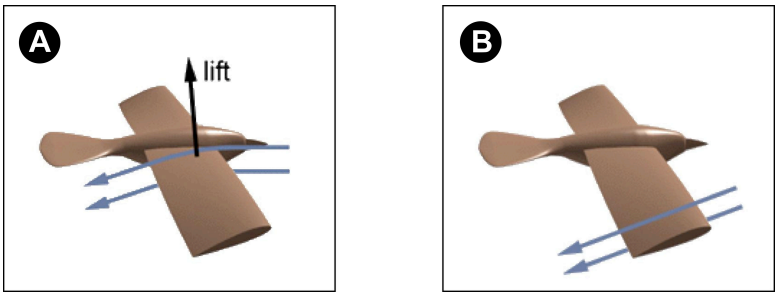

Figure 2.6: *In A, the inner part of the wing produces lift, even during the upstroke. In B, the outer part of the wing is angled to pass through the air with little resistance.*

What we have outlined so far is a basic description of how birds fly, when they are already in the air and cruising along. Birds also have other flying techniques, which they use when taking off or landing, or for other special maneuvers like hovering, as we will see later.

Birds, bats and insects apply a variety of different flapping patterns in hovering and forward flight to generate lift and thrust. Larger birds have relatively simple wingtip paths. For example, an oval tip path is often associated with albatrosses. Smaller flyers exhibit more complicated flapping patterns. Figure 2.7 illustrates some of these patterns for two natural flyers. In figure 2.9, hummingbird's wing lying eight pattern is shown.

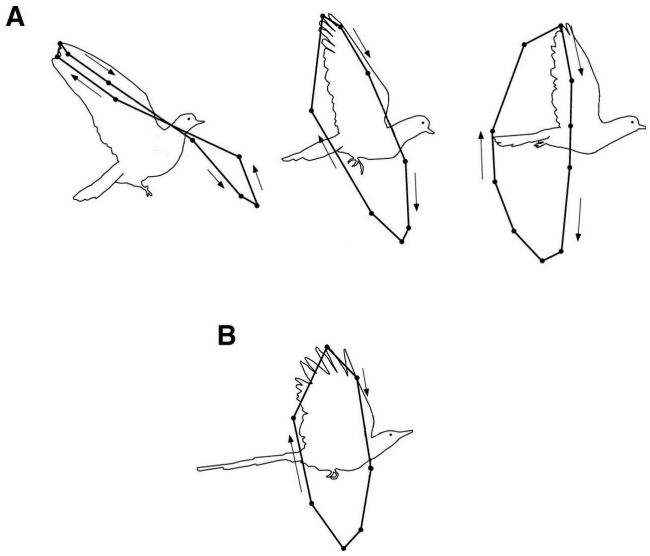

Figure 2.7: *Wingtip paths relative to the body for two natural flyers. (A) Pigeon (Columba Livia), here we see the path transition from tip-reversal upstrokes during slow flight to feathered upstrokes at intermediate speeds and a swept-wing upstroke during fast flight. (B) Black-billed magpie (Pica Hudsonica) wingtip path at all flight speeds [187].*

2.1.3 Hovering

Hovering is used by several species of birds. Hovering, which is generating only lift through flapping alone rather than as a product of thrust, demands a lot of energy. Whether a flying animal can hover or not depends on its size, moment of inertia of the wings, degrees of freedom in the movement of the wings and the wings shape [167]. As a result of these limitations, hovering is mainly performed by small birds and insects. The largest bird able to truly hover is the pied kingfisher, although larger birds can hover but for short periods of time [3, 167, 200].

Large birds can also hover and they do so in an artificial way by flying into a headwind, allowing them to utilize thrust to fly slowly but remain stationary to the ground (or water), this is known as wind-hovering. Kestrels, terns and even hawks use this wind-hovering.

Most birds that hover have high aspect ratio wings that are suited to low speed flying. One major exception to this are the hummingbirds, which are among the most accomplished hoverers among all birds. Hummingbird flight is different from other birds flight in that the wings are fully extended throughout the whole stroke, the stroke being a lying figure eight. Some hummingbirds can beat their wings 52 times a second, though others do so less frequently.

There are two kinds of hovering, symmetric hovering and asymmetric hovering (figure 2.8), as described by Norberg [135] and Shyy [167]. For large birds, which cannot rotate their wings between the forward and backward stroke, the wings are extended to provide more lift during downstroke, whereas during the upstroke the wings are flexed backward to reduce drag. In general the flex is more pronounced in the slow forward flight than in fast forward flight. This type of asymmetric hovering is usually called *"avian stroke"* [9, 167].

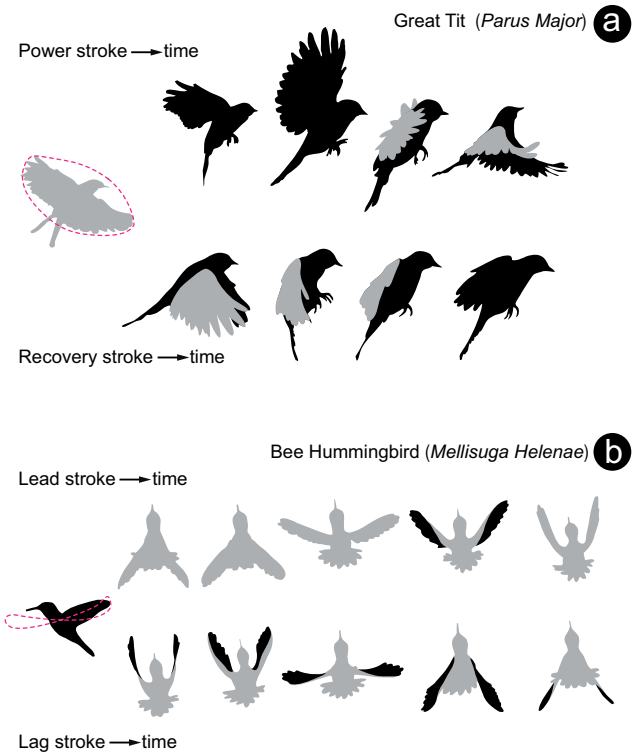

Figure 2.8: *Hovering flight: a) asymmetric hovering or "avian stroke" and b) symmetric hovering or "insect stroke".*

Symmetric hovering, also called normal or true hovering, or *"insect stroke"* [9, 167], is performed by hummingbirds or insects that hover with fully extended wings during the entire wing-beat cycle. Lift is produced during the entire wing stroke, except at the reversal points. The wings are rotated and twisted during the backstroke so that the leading edge of the wing remains the same throughout the cycle, but the upper surface of the wing during the forward stroke becomes the lower surface during the backward stroke. The wing movements during downstroke and upstroke can be seen in figure 2.9. Note that, during hovering, the body axis is inclined at a desirable angle and the wings describe a figure of a lying eight in the vertical plane.

2.1.4 Take-off and landing

Take-off can be one of the most energetically demanding aspects of flight, as the bird needs to generate enough airflow under the wing to create lift. In small birds a jump up will suffice, while for larger birds this is not possible. In this situation, birds need to take a run up in order to generate the airflow to take off. Large birds often simplify take off by facing into the wind, and if they can, perching on a branch or cliff so that all they need to do is drop off into the air.

Landing is also a problem for many large birds with high airspeeds. This problem is dealt with in some species by aiming for a point below the intended landing area (such as a nest on a cliff) then pulling up beforehand. If timed correctly, the airspeed once the target is reached is virtually zero. Landing on water is simpler, and the larger waterfowl species prefer to do so whenever

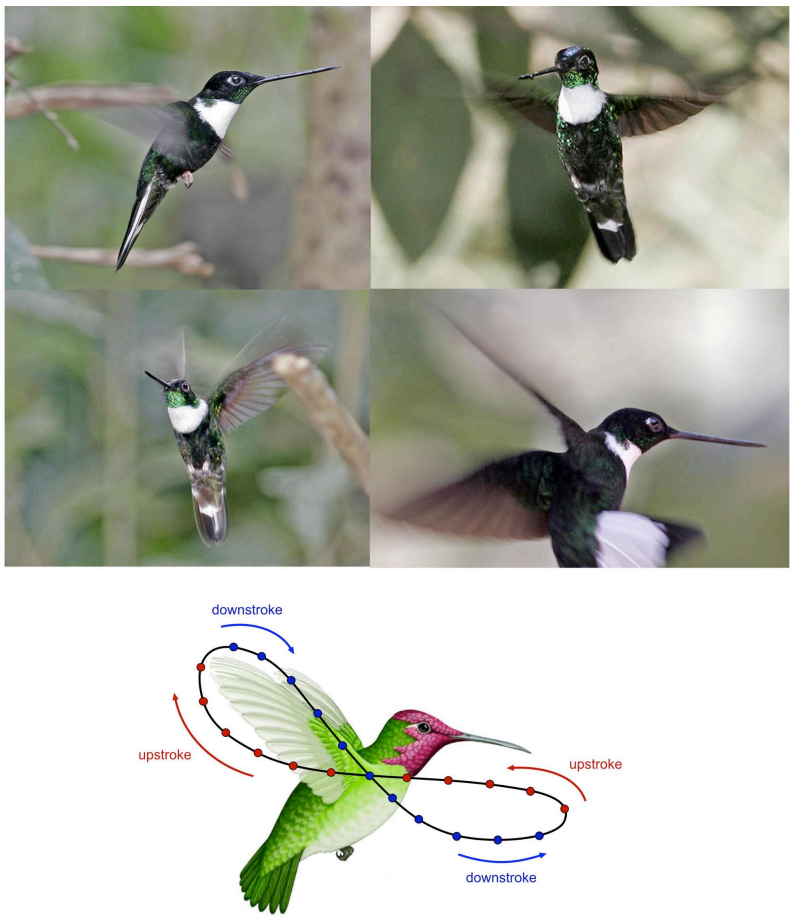

Figure 2.9: *Illustration of a hummingbird in hovering flight. In the bottom figure, hummingbird 's wing figure-eight pattern is shown.*

possible and some species, such as swans, are only able to land on water. In order to lose height and velocity rapidly prior to landing, some large birds such as geese indulge in a rapid alternating series of sideslips in a maneuver termed as whiffling.

2.1.5 Summary

In this section, we just presented a brief overview of flapping flight in nature. In the next sections, we present a review of some of the computational models and experimental observations that constitute our current knowledge on flapping wing propulsion, this followed by a review of nonstationary airfoil aerodynamics (including dynamic stall, leading edge vortex shedding and thrust generation), flapping wing flight in terms of Reynolds number, Strouhal number and reduced frequency and finally we close this chapter with a presentation of flapping wings propulsion performance parameters and kinematics.

Figure 2.10: *A bufflehead running atop the water while taking off.*

Figure 2.11: *Precision touchdown of an eastern imperial eagle on a tree branch.*

2.2 Brief History of Flapping Wing Research: Experimentation, Observations, Analytical and Computational Approaches

For thousands of years, the graceful flight of insects and birds has captivated those who have witnessed it. From those who dream of tasting the freedom of flight in man-made vehicles, to those who hope to further our understanding of some of nature's most fascinating creatures. There is a great variety of documented research in the study of flapping flight, since those studying the topic come from fields such as biology, engineering and aerodynamics. These studies have been undertaken from analytical, experimental and computational standpoints. Hereafter we highlight some of the works which form the basis of our current understanding of flapping flight.

The desire to fly like birds is almost as old as humanity itself. Indeed, Leonardo da Vinci was so

fascinated by the birds flight that he made many sketches of bird's wings and artificial wings and summarized his flapping wing studies in a book manuscript named *"Sul volo degli Uccelli"* [200]. However, little progress was made during the following centuries until Otto Lilienthal, the great pioneer in human flight, began his flying experiments with his brother Gustav in the mid-1800s. While Lilienthal may be most famous for his glider experiments in the 1890s which proved that heavier than air flight is possible without the use of flapping wings, much of his knowledge in aeronautics was derived from experimentation with flapping wings and observation of birds. In 1889, Lilienthal published a book describing his experiments and detailing his predictions for the energy required for flapping wing flight [110]. Perhaps the most significant of his findings was the benefit of using cambered airfoils instead of flat plates, which he discovered by testing models on a rotating apparatus. Shortly after his death in a gliding accident in 1896, Lilienthal served as an inspiration to the Wright brothers in their successful effort to develop powered human flight. Following the sustained flight of the Wright Flyer in 1903 and the subsequent rapid development of fixed-wing airplanes in conjunction with the obvious mechanical complications introduced by flapping wings, the further development of man-made flapping wing vehicles and the research of flapping flight was discouraged.

The earliest scientific theories concerning flapping wing flight pertain to purely heaving airfoils. In independent studies in 1909 and 1912, Knoller [101] and Betz [20], perceived that flapping a wing in a free stream flow resulted in an effective angle of attack (α_{eff}) with a normal force vector containing both lift and thrust components. This phenomenon is now referred to as the Knoller-Betz effect and is illustrated in figure 2.12.

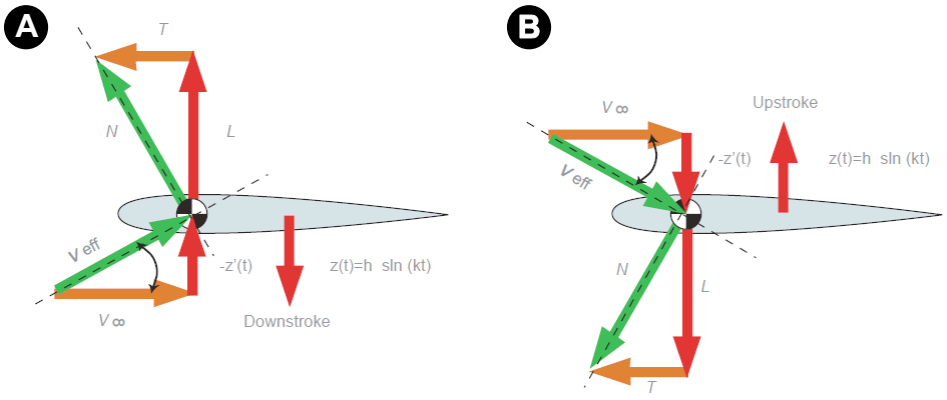

Figure 2.12: *Thrust (T) and lift (L) components of the normal force vector (N) during heaving motion.*

In 1922, Katzmayr [99] conducted wind tunnel tests to validate the Knoller-Betz effect. Rather than flapping the airfoil, Katzmayr sinusoidally oscillated the freestream velocity. Katzmayr's measurements conclusively proved that an airfoil mounted in an oscillating wind stream experienced a thrust force. Also adding to this increasing field of research was Prandtl's student Birnbaum [22], who in the same decade developed a solution for an incompressible flow past flapping airfoils and observed the conditions that lead to flutter or thrust generation. He also suggested the use of a sinusoidally flapping (heaving) wing as an alternative to the conventional propeller.

2.2. BRIEF HISTORY OF FLAPPING WING RESEARCH: EXPERIMENTATION, OBSERVATIONS, ANALYTICAL AND COMPUTATIONAL APPROACHES

By the 1930s, fixed wing aircrafts had improved greatly in performance. At this point, the development of an unsteady aerodynamic theory became important for the investigation of flutter. In 1935, Theodorsen published an analytical approach for estimating the unsteady lift and moment on harmonically oscillating airfoils [184]. In deriving this method, Theodorsen used the assumptions of an inviscid and incompressible flow. He also assumed that all oscillations were of very small amplitude; thus the flow was assumed to remain fully attached to the airfoil during the flapping cycle (the Kutta condition was applied at the trailing edge of the airfoil). Theodorsen assumed that the wake of the airfoil would take the form of a continuous vortex sheet of sinusoidally varying strength, stretching from the trailing edge to infinity in the downstream direction. The wake was not allowed to change shape in response to the velocity induced by the wake. This Theodorsen's theory will become in the years to come the standard tool to analyze airfoil flutter, rotorcraft aerodynamics and flapping flight problems.

In the following decade, the aerodynamics of heaving-and-pitching airfoils received much attention because of its importance for reliable flutter and gust response analyses. However, such analyses require only the determination of the lifting forces generated by heaving or pitching airfoils, and consequently, little effort was devoted over the years to the determination of the thrust forces.

Nevertheless, in the mid 1930s von Karman and Burgers [205] offered the first theoretical explanation of drag or thrust production based on the observed location and orientation of the wake vortices, as illustrated in figure 2.13. In their work, von Karman and Burgers [205] experimentally observed that a wake consisting of two rows of counter-rotating vortices could produce a thrust force on an airfoil in an incompressible flow. At about the same time, Garrick [57] applied Theodorsen's inviscid, incompressible, oscillatory, flat plate theory [184] to the determination of the thrust force (which remains the classical reference work to this day) and showed that heaving airfoils generate thrust over the whole frequency range considered, whereas pitching airfoils do so only with frequencies above a certain critical value and as function of the pivot location. The first experimental verification of Garrick predictions was provided by Silverstein and Joyner [168] in 1939. Later on, in 1950, Bratt [23] performed flow visualization experiments that corroborated von Karman and Burger's observations. Of particular interest, Bratt's experimental data include several cases where a non-symmetrical, deflected wake pattern was observed, but no comment was made on these deflected wakes.

Recognizing the fact that some of the flapping energy is lost in the form of vorticity shed in the wake, Schmidt [161] proposed that a stationary wing be placed in the oscillatory wake of a flapping wing to take back some of the vortical energy lost by the flapping airfoil, the aft wing thus is exposed to an oscillatory flow which generates thrust by virtue of the Katzmayr effect. Schmidt, as a result of his studies about flapping foils in the 1940s and 1950s, developed the wave propeller (which he claimed achieved efficiencies as good as those of conventional propellers) and demonstrated it on a catamaran boat.

In the early 1970s, Lighthill [109] performed a very similar analysis to that of Garrick [57], with an additional assumption of pitching motion leading plunging motion by 90 degrees, in the context of lunate (crescent-shaped) tail propulsion by fishes and cetaceans. Using an energy method, he obtained expressions for thrust and propulsive efficiency that are identical to those of Garrick when converted into similar terms. In principle, any other relative phase difference between pitching and plunging motion may be accounted for, by a change in the pitch axis of the airfoil,

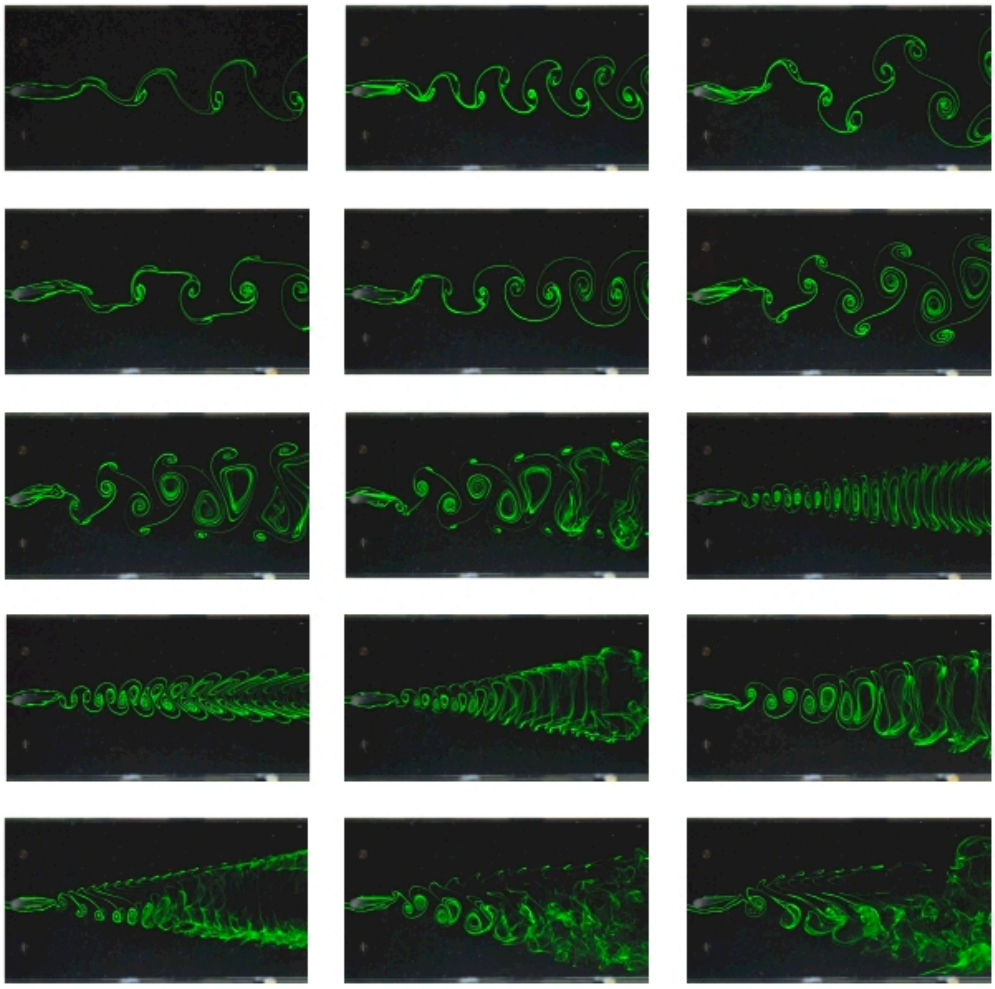

Figure 2.13: *Dye visualizations of different wakes behind an oscillating airfoil (from von Karman vortex street, to neutral wake, to reverse von Karman vortex street, to deflected wake).*

however this is strictly only true for very small amplitude motion. As the Garrick work makes no assumption about relative phases of plunging and pitching, Lighthill work it is slightly more general. Similar analyses of the small amplitude motion of a $2\mathbb{D}$ flat plate in potential flow may be found in a variety of sources (*e.g.*, Ashley and Landahl [8] and Katz and Plotkin [98]).

The linearized potential flow analyses discussed above, particularly the Garrick analysis, contain a number of assumptions about the flow, the airfoil geometry and the airfoil motion. Firstly, the airfoil is assumed to be thin and is treated as a flat plate. Secondly, the flow is assumed to be inviscid and incompressible, and the Kutta condition is applied to the flow at the trailing edge of the airfoil. Finally, the motion of the airfoil is assumed to be of small amplitude and the wake does not evolve in response to its own induced velocity field. In order to avoid the limitations imposed by the previous assumptions and to improve the predictive capabilities, new computational models that account for the unsteady nature of the motion, arbitrary airfoil sections and three-dimensional effects were developed.

Of special note is the replacement of Theodorsen oscillatory thin-airfoil theory by an approach which enables the computation of incompressible potential flow past oscillating airfoils of arbitrary shape. This is being accomplished by the placement of sources and vortices on the airfoil surface rather than along the chord line. This so-called panel method was pioneered by Giesing [58], who generalized the method of Hess and Smith [82], for steady airfoil flow. The method was further developed by Teng [183], Platzer *et al.* [148], and Jones *et al.* [147]. More recently, two-dimensional unsteady panel methods have been used for prediction of flapping wing MAV propulsion [94, 96, 97]. Three-dimensional methods also have been used to predict the forces on insect wings and cetacean tails [171, 173].

Inviscid analyses require the separation point of the flow on the airfoil or wing to be known ahead of time. This is usually fixed at the trailing edge (the Kutta condition), and vorticity is shed into the wake from this point. Navier-Stokes flow solvers avoid this limitation by using the full viscous flow equations rather than potential flow, allowing flow separation and vortex shedding to be predicted rather than assumed *a priori*, allowing simulation of flows that involve leading and trailing edge separation. Also, thanks to the rapid increase in computer power over the past few years, such viscous flow solvers are becoming more popular and have been successfully used to model flapping wing aerodynamics, thus making possible to compute the strong viscous effects and three-dimensional flows characteristics of flapping flight.

Some recent works using Navier-Stokes solvers that are worth to mention, include the work done by Young and Lai [216], where it is shown that the vortical wake structures, and the lift and thrust characteristics of a heaving airfoil are strongly dependent on the oscillation frequency and amplitude. Isogai *et al.* [89] carried out Navier-Stokes computations for a single flapping airfoil. They calculated the thrust and the propulsive efficiency for various combinations of frequency and phase shift, and gave a detailed analysis of the effects of the dynamic stall phenomena on the behavior of the thrust and the propulsive efficiency. In a following work about the aerodynamic performance of a dragonfly, Isogai *et al.* [88], clarified the fundamental mechanism of the hovering flight of a dragonfly. Another flow simulation of an insect was presented by Togashi *et al.* [189] in which, by solving the Navier-Stokes equations, they gave the approximate numerical simulation of the flow past a hornet in a forward flight. Liu *et al.* [112], using a $3\mathbb{D}$ Navier-Stokes solver, successfully modeled the powered hovering mode of a Hawkmoth. Lewin and Haj-Hariri [108] and Wang [207], both examined the propulsive characteristics of an elliptical airfoil heaving sinusoidally over a range of frequencies and heave amplitudes in order to correlate viscous flow structures to thrust generation. Pedro *et al.* [140], numerically studied the propulsive efficiency of a flapping hydrofoil at a Reynolds number of 1100. In their work, Pedro *et al.* [140] studied airfoils undergoing pure pitching motion and combined pitching-and-heaving motion and they showed the sensitivity of thrust and efficiency to the Strouhal number, maximum pitch angle and phase angle. Hover *et al.* [87] used sinusoidal and non-sinusoidal effective angle of attack variations in time to investigate the propulsive performance of an airfoil undergoing combined heave and pitch oscillations. Lee *et al.* [106] identified the key physical flow phenomenon dictating the thrust generation of a heaving and/or pitching airfoil in terms of flow and geometry parameters. Tuncer *et al.* [196, 197, 198] performed several Navier-Stokes computations to explore the effect of flow separation on the thrust and the propulsive efficiency of a single flapping airfoil in combined pitch and heave oscillations.

Experimentally, Jones *et al.* [94] and Lai and Platzer [105], conducted water tunnel flow visualization experiments on flapping airfoils which have provided a considerable amount of information on

the wake characteristics of thrust producing flapping airfoils. Koochesfahani [103] experimentally studied the wake structure behind a flapping foil and found different topologies of the wake with associated numbers of shed vortices per cycle of oscillations as function of the amplitude and the frequency of flapping. Triantafyllou *et al.* [191], based on the experimental results of Koochesfahani [103] and on a linear stability analysis of an average velocity profile, assumed that optimal efficiency is obtained when an airfoil flaps at the frequency of maximum spatial amplification of the wake. Anderson *et al.* [7], in their experiments, also observed that the phase angle between pitch and heave oscillations plays a significant role in maximizing the propulsive efficiency. The experimental studies by Jones *et al.* [95] and Platzer and Jones [146] demonstrated that two airfoils arranged in a biplane configuration and oscillating in counter-phase show significant benefits of thrust and propulsive efficiency compared to a single flapping airfoil.

More recently, Heathcote and Gursul [67] carried out water tunnel experiments on a heaving-and-pitching flexible airfoil for low Reynolds numbers. They observed a peak in thrust coefficient at a particular value of the phase shift between heaving and pitching for fixed heave and pitch amplitudes. Schouveiler *et al.* [163] experimentally studied the performance of an aquatic propulsion system inspired from the thunniform swimming mode to investigate the effects of flapping parameters on the thrust force and the hydro-mechanical efficiency. In the computational area of flexible airfoils/fins, Miao and Ho [124], studied the effect of chordwise flexure amplitude on the unsteady aerodynamic characteristics for flapping airfoils with various combinations of Reynolds number and reduced frequency. In this study, they observed an enhancement in the propulsive efficiency for a flapping airfoil with flexure amplitude of 0.3 of the chord length, they also found that the flow conditions which yield the highest propulsive efficiency correspond to a Strouhal number St of 0.255. Liu and Kawachi [113], performed a numerical study of the undulatory locomotion of a swimming body. They successfully modeled the unsteady hydrodynamics of a realistic three-dimensional tadpole-shaped model, establishing the importance of accurately predicting a staggered array of reverse von Karman vortices, the jet stream and their correlation with thrust generation. They also pointed to an optimal propulsive mechanism appropriate to undulatory swimming, which is achieved by a best coupling of the geometry and the motion matched to the body.

Despite the potential of flapping wings for either pure propulsion or as an integrated lift/propulsion system, it was regarded as unattractive until very recently. Flapping wing studies therefore largely remained restricted to scientists interested in bird flight or fish propulsion problems. An unexpected revival of interest in the study of flapping wing flight phenomena occurred in the late 1990s with the announcement of a major initiative by the United States of America Defense Advanced Research Projects Agency (DARPA) to encourage the development of micro-air-vehicles (MAVs). The goal of the DARPA MAVs program was to determine whether evolving technologies could be favorably integrated into a mission capable flight system for military surveillance and reconnaissance applications. The only requirement was that the dimension of the vehicle should not exceed 15 cm. There were no other restrictions on the design. The use of flapping wings for vehicles with dimensions not exceeding 15 cm in length or span is an obvious option because of the low efficiency of conventional propellers and fixed wings at low Reynolds number. Therefore, this DARPA initiative sparked a large number of investigations in the field of flapping wing propulsion; some of these investigations are compiled in [127].

2.3 The Physics of Drag and Thrust Generation Due to Wing Flapping

As already mentioned, Knoller [101] and Betz [20] were the first ones to offer an explanation for the birds' ability to generate a propulsive force by means of flapping their wings. Consider the airfoil undergoing sinusoidal flapping while also flying forward. As the airfoil moves through its mean position during the downward stroke, it is effectively exposed to a flow with positive angle of incidence (see figure 2.12). Similarly, it sees a negative incidence angle during the upstroke. If, for simplicity, the resulting aerodynamic force is assumed to be essentially perpendicular to the instantaneous approach flow angle, then decomposition into a force component parallel to the flight velocity vector will produce a small sinusoidally varying thrust force. It is understood that this explanation is greatly simplified. The actual flow which is produced is considerably more complicated.

The flow over a stationary airfoil or a bluff body at low Reynolds number produces a von Karman vortex street as shown in figure 2.14. In this configuration, where the upper row of vortices rotates clockwise and the lower row counterclockwise (for flow from left to right), the measured time-averaged velocity distribution in the wake shows a distinct velocity or momentum deficit, indicative of drag. This vortex configuration is hereafter referred as drag producing wake.

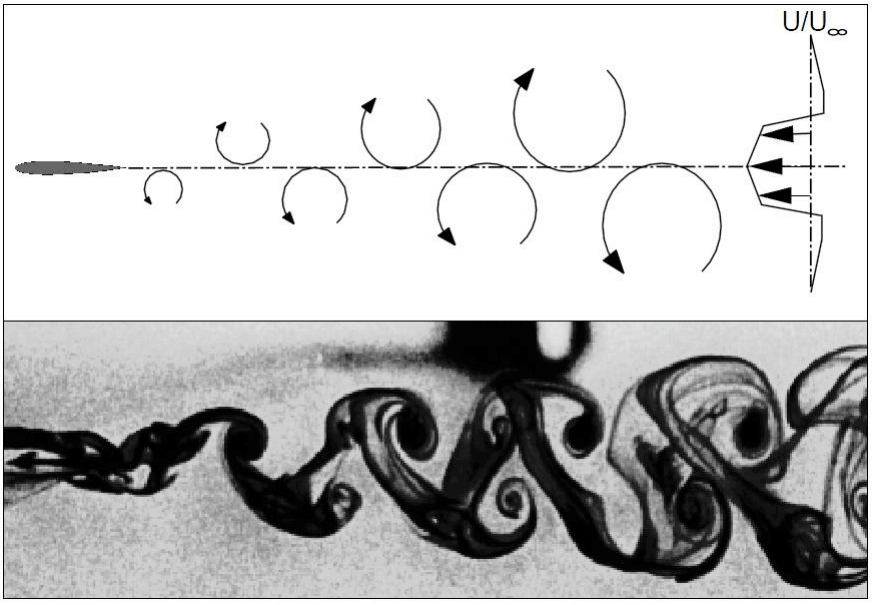

Figure 2.14: *Vortex street indicative of drag production (drag producing wake) [93].*

As is well known, every change in the incidence of the airfoil will produce a starting vortex which is shed from the trailing edge. Therefore, a sinusoidally oscillating airfoil will generate a vortex street behind the airfoil. This phenomenon can be reproduced easily experimentally or simulated with the computational approaches highlighted in the previous section. Depending of the heave velocity, the resulting vortex street can be drag producing wake or can consist of an upper row of counterclockwise vortices and a row of lower clockwise vortices (see figure 2.15). This vortex street therefore is just the opposite of the well known von Karman vortex street and is known

as reverse von Karman street. If time-averaging is applied at some location cutting the wake in the normal direction to the free-stream a jet profile or momentum surfeit wake is obtained. The vortex street produced by the flapping foil in effect produces a jet flow. This vortex configuration is hereafter referred to as thrust producing wake. This is to be expected since the thrust experienced by the airfoil must be found as momentum increase in the fluid. As shown by Jones *et al.* [94] and Lewin and Haj-Hariri [108], this jet flow can indeed be measured and is in good agreement with panel code and Navier-Stokes solver predictions.

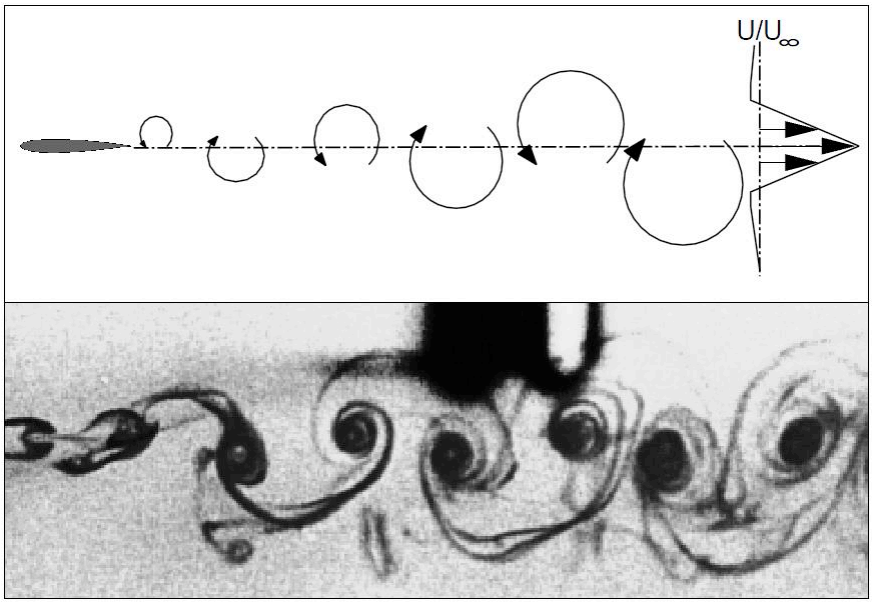

Figure 2.15: *Vortex street indicative of thrust production (thrust producing wake) [93].*

From this analysis, clearly we see that increasing the vertical spacing between the rows increases the region of lower time-averaged velocity (for von Karman street) or higher velocity (for reverse von Karman street) between the rows. This then increases the drag (or thrust) of the configuration in the direct proportion to the vertical spacing. It follows that reducing the vertical spacing to zero, so that the two vortex rows are interspersed as in figure 2.16, will result in zero net drag or thrust production. This vortex configuration is hereafter referred to as neutral wake.

Jones *et al.* [93], found that for large plunge velocities, the symmetric vortex street changes into a dual-mode or nonsymmetric vortex street, as show in figure 2.17. In this case, in addition to a net thrust, a net lift is also observed according to the deflection of the vortex street. This vortex configuration is hereafter referred to as deflected wake or lift-thrust producing wake. This phenomena was previously observed by Bratt in 1950 [23], but he did not make any comments on these deflected wakes. Once again, the flow visualizations are in good agreement with panel code [94, 96, 171] and Navier-Stoke solver [108, 115] predictions.

This encouraging agreement between the measurements and the inviscid flow predictions of Jones *et al.* [93, 147] and Platzer *et al.* [148], might give the impression that the physics of flapping airfoils is understood reasonably well and that the prediction of the achievable thrust can be made with considerable confidence by using inviscid methods. Unfortunately, even disregarding

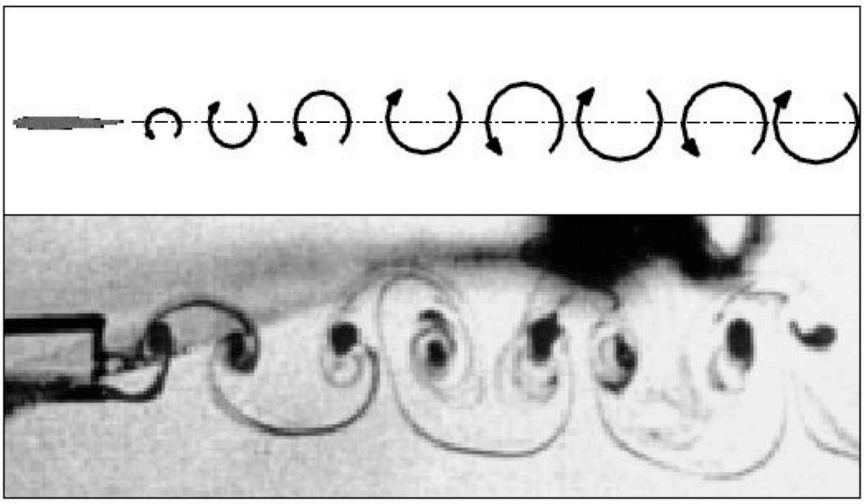

Figure 2.16: *Vortex street indicative of zero drag (neutral wake) [93].*

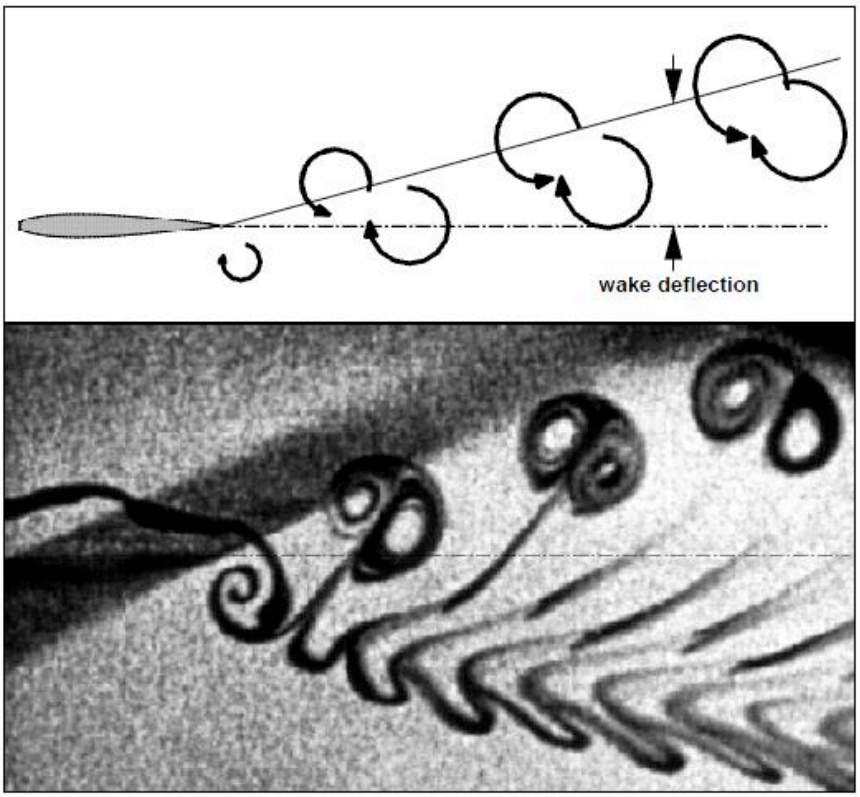

Figure 2.17: *Dual-mode or nonsymmetric vortex street indicative of thrust and lift production (deflected wake) [93].*

the three-dimensional flow effects introduced by finite-span wings, the range of validity of inviscid flow predictions is severely limited by the onset of dynamic stall. This seems to be particularly true at the low Reynolds numbers typically required for micro-air-vehicles. Hence panel methods

must be dropped in favor of more sophisticated Navier-Stokes solvers, which take into account viscous effects.

2.4 The Phenomenon of Dynamic Stall and Leading Edge Vortex (LEV) Shedding

Dynamic stall is a non-linear unsteady aerodynamic effect that occurs when airfoils rapidly change the angle of attack. The rapid change can cause a strong vortex to be shed from the leading edge of the airfoil, and travel backwards above the wing, strongly interacting with the vortex which forms at the trailing edge. The vortex, containing high velocity airflows, briefly increases the lift produced by the wing. As soon as it passes behind the trailing edge, however, rapid lift loss and changes in pitching moment occur, leading to a severe hysteresis loop in lift, drag and pitching moment.

Dynamic stall is an effect mostly associated with helicopters, turbines, windmill blades and recently to flapping wing propulsion. Helicopter aerodynamicists are quite familiar with this phenomenon. A helicopter blade in forward flight can experience dynamic stall while it is in the so-called retreating blade position, exposing the blade to high incidence angles. For this reason, the aerodynamics of pitching airfoils experiencing dynamic stall has been studied to a considerable extent both experimentally and computationally. The current state-of-the-art can be found in the papers of Carr and Chandrasekhara [31], Ekaterinaris and Platzer [47], McCroskey *et al.* [117] and Rozhdestvensky and Ryzhov [156].

Most dynamic stall studies have been limited to pitching airfoils because of the importance of this motion for helicopter blades. However, for thrust generation it is well known (and has been shown in detail by Jones and Platzer [97]) that pure heave or a combined pitch/heave motion is required in order to produce significant thrust forces. Very few experiments involving dynamic stall due to pure heave have been carried out, but several Navier-Stokes computations have been reported by Isogai *et al.* [89], Tuncer and Platzer [198] and Ramamurti and Sandberg [151], among others. These computations clearly show the possibility of occurrence of dynamic stall for values of flapping frequency, amplitude, and Reynolds number typical for MAV flight.

The basic physics of dynamic stall is illustrated in figure 2.18, where a sequence of images during the downstroke of a heaving airfoil is shown from a Navier-Stokes simulation of a NACA 0012 airfoil undergoing sinusoidal heaving motion. In the figure, a strong vortex forms near the leading edge (LEV), propagates over the upper surface and is then swept downstream past the trailing edge. While the vortex is over the airfoil upper surface, lift is enhanced. This increased lift is significantly greater than the static lift which would be generated at the corresponding static incidence angle. As soon as the vortex approaches the trailing edge this lift is reduced quite suddenly and dramatically. While the presence of dynamic stall is generally adverse on aircrafts and rotorcrafts, there is evidence that birds and insects may benefit from this effect as a high-lift mechanism, by simple relying on leading edge vortices (LEV) created by dynamic stall during the flapping motion [48, 107, 125]. Basically, LEVs are originated due to roll up of the shear layer separating from the leading edge region of the wing during flapping or pitching motion.

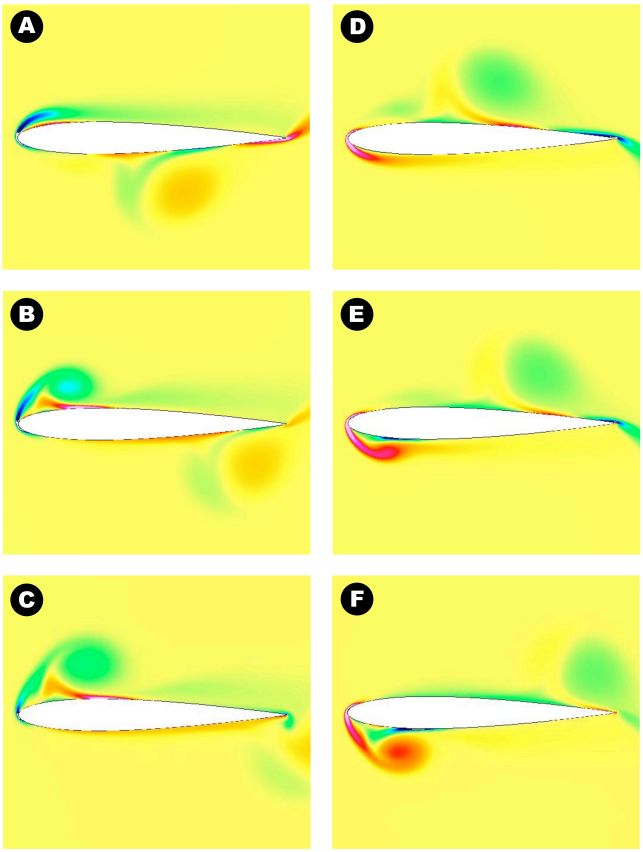

Figure 2.18: *Dynamic stall on a heaving airfoil during downstroke (sequence is top-to-bottom left column, then top-to-bottom right column).*

2.5 Reynolds Number in Terms of Flapping Flight

Given a reference length L_{ref} and a reference velocity U_{ref}, one normally defines the Reynolds number Re as

$$Re = \frac{\rho U_{ref} L_{ref}}{\mu} = \frac{U_{ref} L_{ref}}{\nu} \tag{2.1}$$

where ρ is the fluid density, μ is the dynamic viscosity of the fluid and ν is the fluid kinematic viscosity. Re represents the fluid ratio of inertial forces to viscous forces and is commonly used in fluid dynamics. In flapping flight, with consideration of the fact that flapping wings produce lift and thrust, the mean wing's chord length c_m is used as the reference length L_{ref}, whereas the body length or averaged length of the caudal fin is typically used in swimming animals. The reference velocity U_{ref} is also defined differently in hovering and forward flight.

In hovering flight, as there is no forward velocity, the mean wingtip velocity may be used as the reference velocity, which can be written as $U_{ref} = \omega R$, where R is the wing length (half wingtip-to-wingtip span) and ω is the mean angular velocity of the wing ($\omega = 2\Phi f$, where Φ is the wing-beat amplitude, measured in radians, and f is the flapping frequency). Therefore the

Reynolds number for a 3𝔻 flapping wing in hovering flight (Re_{fh3}) is given by

$$Re_{fh3} = \frac{U_{ref}L_{ref}}{\nu} = \frac{2\Phi f R c_m}{\nu} = \frac{\Phi f R^2}{\nu}\left(\frac{4}{\mathrm{AR}}\right) \tag{2.2}$$

where AR is the wing aspect ratio ($\mathrm{AR} = S^2/A$) which gives a relation between the wingspan S and the wing area A. In eq. 2.2, the aspect ratio is introduced in the form $\mathrm{AR} = (2R)^2/A$ with the wing area being the product of the wing span ($2R$) and the mean chord (c_m). Note that the Reynolds number here is proportional to the wing-beat amplitude Φ, the flapping frequency f, the square of the wing length R^2, but inversely proportional to the AR of the wing.

For a 2𝔻 flapping airfoil undergoing hovering motion, the Reynolds number (Re_{fh2}) is defined by the maximum heaving velocity, such as

$$Re_{fh2} = \frac{\rho U_{ref}L_{ref}}{\mu} = \frac{U_{ref}L_{ref}}{\nu} = \frac{2\pi f h_a c}{\nu} \tag{2.3}$$

where f is the flapping frequency, h_a is the heaving amplitude, and c is the airfoil chord length.

In forward flight, for both 2𝔻 and 3𝔻 applications, the forward velocity U is often used as the reference velocity U_{ref} and the mean chord length c_m as the reference length L_{ref}, hence eq. 2.1 is solely used to obtain the forward flight Reynolds number Re. Compared with the hovering flight Reynolds number, which is proportional to R^2, the forward flight Reynolds number is proportional to R.

2.6 Strouhal Number and Reduced Frequency

A fundamental dimensionless parameter in flows showing an unsteady aerodynamic nature is the Strouhal number (St), this number is well known for characterizing the vortex dynamics and shedding behavior of unsteady flows. In some St ranges, the flapping airfoil produces thrust, and the vortices in the wake are termed reverse von Karman vortices. In general, for flapping flight, the dimensionless parameter St is normally defined as

$$St = \frac{fL_{ref}}{U_{ref}} = \frac{2fh_a}{U_{ref}} \tag{2.4}$$

where f is the stroke (flapping) frequency in flapping flight, h_a is the stroke (flapping) amplitude, and U is the forward velocity. This definition describes a ratio between the oscillating (flapping) speed (fh_a) and the forward speed (U), which offers a measure of propulsive efficiency in flying and swimming animals. In the study of natural flyers and swimmers in cruising condition it is found that the Strouhal number, as defined by eq. 2.4, is often within a region of $0.2 < St < 0.4$; in this range of St, the propulsive efficiency (see eq. 2.20) is high, with an optimal St value of 0.3 [136, 182, 192].

Another dimensionless parameter that characterizes the unsteady aerodynamics of pitching and heaving airfoils is the reduced frequency, which is a measure of the residence time of a particle convecting over the airfoil chord compared to the period of motion. The reduced frequency k is

defined as

$$k = \frac{2\pi f L_{ref}}{2U_{ref}} = \frac{\pi f c_m}{U_{ref}} = \frac{\omega c_m}{2U_{ref}} \tag{2.5}$$

where ω is equal to $2\pi f$. In hovering $3\mathbb{D}$ flight, for which there is no forward speed, the reference speed U_{ref} is defined as the mean wingtip velocity $2\Phi f R$; then the reduced frequency k_{fh3} can be formulated as

$$k_{fh3} = \frac{\pi f c_m}{U_{ref}} = \frac{\pi c_m}{2\Phi R} = \frac{\pi}{\Phi \mathrm{AR}} \tag{2.6}$$

where the AR is introduced here again as in eq. 2.2. For the special case of $2\mathbb{D}$ hovering airfoils, the reference velocity U_{ref} is the maximum flapping velocity (see eq. 2.3), and the reduced frequency k_{fh2} is defined as

$$k_{fh2} = \frac{\pi f c}{U_{ref}} = \frac{c}{2h_a} \tag{2.7}$$

which is simply related to the normalized stroke amplitude.

The Strouhal number St (eq. 2.4), may be related to the reduced frequency k (eq. 2.5) as follows

$$St = \frac{f L_{ref}}{U_{ref}} = \frac{2f h_a}{U_{ref}} = \frac{1}{\pi}\frac{\omega c_m}{2U_{ref}}\frac{2h_a}{c_m} = \frac{k}{\pi}\frac{2h_a}{c_m} = \frac{2}{\pi}\frac{k h_a}{c_m} = \frac{2}{\pi}kh \tag{2.8}$$

where h is the nondimensional heaving amplitude equal to h_a/c_m and where the product kh is defined as the maximum nondimensional heaving velocity.

In the case of forward flight, another dimensionless parameter is the advance ratio J. In a general $2\mathbb{D}$ or $3\mathbb{D}$ framework, J is defined as

$$J = \frac{U_{ref}}{2\pi f h_a} \tag{2.9}$$

which is related to St, specifically, $J = 1/(\pi St)$. In eq. 2.9, the reference velocity U_{ref} is the forward-flying velocity U.

2.6.1 Strouhal Number as the Fundamental Aerodynamic Parameter in Flapping Flight

In studying natural flyers and swimmers and in designing a lifting and/or propulsive man-made vehicle based on flapping wings, an immediate question is the range of flapping parameters that may be chosen to optimize the design thrust, efficiency, or other criteria. Evolution is not guaranteed to find a solution that is globally optimized among the range of available parameters, and nature may be more limited in the range of parameters to change. However, a thorough examination of nature's techniques is a logical starting point in defining guiding principles.

Taylor *et al.* [182] performed a study of published wing beat frequencies and amplitudes and cruise speeds, across a range of birds, bats and insects, to determine Strouhal numbers in cruising flight.

They found 75% of the 42 species considered to fall within a narrow range of $0.19 < St < 0.41$, with a mean value of $St = 0.29$. They made the point that whilst similar species might be expected to exhibit similar Strouhal number due to similar morphological and physiological characteristics, the disparate variety of species used in their study (spanning five orders of magnitude of body mass) strongly implies that the narrow Strouhal number range is due to aerodynamic principles alone.

Triantafyllou *et al.* [193], provided a graph of measured Strouhal numbers for a range of fishes, sharks and cetaceans, with all falling largely within the Strouhal number range of $0.25 < St < 0.35$. In a later study, Triantafyllou *et al.* [191] expanded on these results, showing that this narrow range of selected Strouhal number holds over a Reynolds number range of $10^4 < Re < 10^6$, with the Re based on the averaged length of the caudal fin (tail) in the specimens examined. The velocities used in the calculation were stated to be at or near maximum velocity range for each species.

Nudds *et al.* [136], proposed a simple and accurate empirical model for predicting wing-beat frequency in birds, based on the Strouhal number. The proposed aerodynamic model predicted wing-beat frequency better than any other relationship proposed, explaining 90% of the observed variance in a sample of 60 birds species. In the results presented by Nudds *et al.*, they found that their calculations were consistent with the hypothesis that birds have converged upon a narrow optimum range of St in cruising flight. The best estimates of St for the empirical data given by them fell within the range of $0.2 < St < 0.4$ associated with high propulsive efficiency in other theoretical and experimental studies [152, 193]. These results lead Nudds *et al.* to conclude, *"Avian wing kinematics therefore appear to have been tuned by natural selection for high aerodynamic efficiency"*.

These results all support the proposition that the Strouhal number is the single, or at least the dominant parameter that controls the aerodynamics of flapping flight, insofar as high efficiency propulsion is concerned [108, 136, 182, 191, 192, 193, 207]. As stated by Taylor [182], *"The exact mechanism by which St controls the efficiency of force production has yet to be fully elucidated, but is generally thought to reflect the role of St in governing the time-scales of vortex growth and shedding"*.

Hence, throughout this dissertation the Strouhal number St (or equivalently the product kh according to eq. 2.8) will be used as the fundamental aerodynamic parameter when characterizing the flapping motion, unless otherwise specified.

2.7 Flapping Airfoils Performance Parameters

In the study of flapping airfoils, several parameters may be used to quantify the flow characteristics. Hereafter, we present the most representative ones. Two parameters that provide important information in the study of flapping wing propulsion are drag and lift coefficients, which are defined as follow

$$c_d = \frac{D}{\frac{1}{2}\rho U^2 c} \tag{2.10}$$

$$c_l = \frac{L}{\frac{1}{2}\rho U^2 c} \tag{2.11}$$

Since we are studying flapping wing propulsion, it is more convenient to think in terms of thrust instead of drag. Hence, thrust can be seen as the opposite in direction to the drag force (but equal in magnitude), therefore we obtain

$$c_t = -c_d = \frac{T}{\frac{1}{2}\rho U^2 c} \tag{2.12}$$

In equations 2.10, 2.11 and 2.12; D, L and T are the drag forces, lift forces and thrust forces (same as drag forces but opposite in sign), respectively; ρ is the fluid density, U is the forward velocity and c is the airfoil chord.

The instantaneous power input P, can be defined as the amount of energy imparted to the airfoil for it to overcome the fluid forces and is equal to

$$P(t) = -L(t) \times \dot{y}(t) - M(t) \times \dot{\alpha}(t) \tag{2.13}$$

where $\dot{y}(t)$ is the vertical velocity of the airfoil pivot point ($\dot{y}(t) = \frac{d}{dt}y(t)$), $y(t)$ is the plunging motion of the airfoil pivot point, $\dot{\alpha}(t)$ is the angular velocity of the airfoil about the pivot point ($\dot{\alpha}(t) = \frac{d}{dt}\alpha(t)$), $\alpha(t)$ is the pitching motion of the airfoil about the pivot point, and $M(t)$ is the moment created by the lift and drag forces at the pitching axis and is nondimensionalized by

$$c_m = \frac{M}{\frac{1}{2}\rho U^2 c^2} \tag{2.14}$$

In eq 2.13, the sign of both terms is negative as the lift force and the moment are reaction forces created by the fluid as the airfoil moves through it, where the products $L(t) \times \dot{y}(t)$ and $M(t) \times \dot{\alpha}(t)$ are the instantaneous supplied energy for vertical translation motion (heaving) and angular motion (pitching), respectively. The input power can be also nondimensionalized as follows

$$c_P = \frac{P}{\frac{1}{2}\rho U^3 c} \tag{2.15}$$

Power, thrust, lift and moment coefficients can be also averaged over time as

$$c_{P_{mean}} = \overline{c_P} = \frac{1}{\mathbb{T}} \int_t^{t+\mathbb{T}} C_P(t) dt \tag{2.16}$$

$$c_{t_{mean}} = \overline{c_t} = \frac{1}{\mathbb{T}} \int_t^{t+\mathbb{T}} C_T(t) dt \tag{2.17}$$

$$c_{l_{mean}} = \overline{c_l} = \frac{1}{\mathbb{T}} \int_t^{t+\mathbb{T}} C_L(t) dt \tag{2.18}$$

$$c_{m_{mean}} = \overline{c_m} = \frac{1}{\mathbb{T}} \int_t^{t+\mathbb{T}} C_M(t)dt \tag{2.19}$$

where $\mathbb{T}$ is the period of flapping motion and is equal to $\mathbb{T} = 2\pi/\omega$. Finally, the propulsive efficiency can be seen as a measure of the energy lost in the wake versus the energy used in creating the necessary thrust, and is given by

$$\eta = \frac{T_{mean}U}{P_{mean}} = \frac{c_{t_{mean}}}{c_{P_{mean}}} = \frac{\overline{c_t}}{\overline{c_P}} \tag{2.20}$$

2.8 Airfoil Geometry and Flapping Kinematics

For a generic 2$\mathbb{D}$ case, the airfoil geometry and airfoil motions are shown in figure 2.19. Vertical (heaving) and rotational (pitching) motions are shown. Horizontal motion (lagging or surging) will be not considered for 2$\mathbb{D}$ cases. Note that throughout this dissertation single-mode motions will be referred to as pure pitching or pure heaving, whereas the term flapping will imply a combination of heaving-and-pitching in 2$\mathbb{D}$.

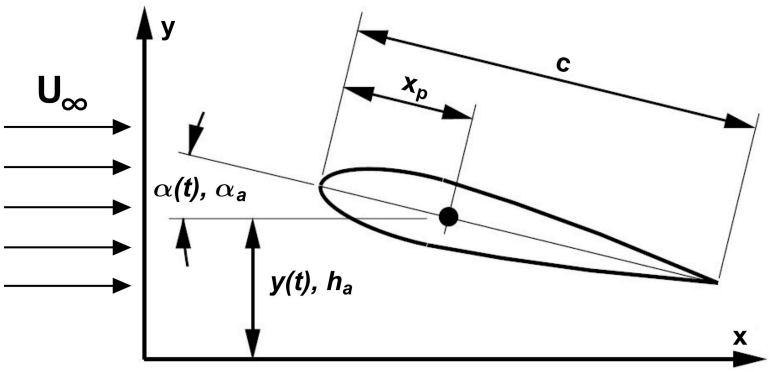

Figure 2.19: *Airfoil geometry and airfoil motion. In the figure, heaving motion $y(t)$ of the pivot point, pitching motion $\alpha(t)$ of the airfoil about the pivot point, maximum heaving amplitude h_a, maximum pitching amplitude α_a, airfoil chord c, pivot point x_p and free-stream velocity U_∞ are shown.*

In figure 2.19, c is the airfoil chord, x_p is the distance from the leading edge to the pivot point which simultaneously translates vertically (heave), h_a is the maximum heaving amplitude, α_a is the maximum pitching amplitude, $y(t)$ is the heaving motion and $\alpha(t)$ is the pitching motion.

The 2$\mathbb{D}$ kinematics of the airfoil undergoing a combination of time-dependent heaving ($y(t)$) and pitching ($\alpha(t)$) motions, can be describe by symmetric, periodic, harmonic functions as follows

$$y(t) = h_a cos(\omega_h t + \varphi_h) = h_a cos(2\pi f_h t + \varphi_h) \tag{2.21}$$

$$\alpha(t) = \alpha_a cos(\omega_\alpha t + \varphi_\alpha) = \alpha_a cos(2\pi f_\alpha t + \varphi_\alpha) \tag{2.22}$$

where h_a is the heaving amplitude and is defined positive upwards, α_a is the pitch amplitude and is defined positive clockwise, ω_h is the heaving angular frequency ($\omega_h = 2\pi f_h$), f_h is the heaving oscillating frequency, ω_α is the pitching angular frequency ($\omega_h = 2\pi f_\alpha$), f_α is the pitching oscillating frequency, φ_h is the phase angle of the heaving motion and φ_α is the phase angle of the pitching motion.

Based on the definition of reduced frequency eq. 2.18, the airfoil kinematics eq. 2.21 and eq. 2.22 can be rewritten as

$$y(t) = h_a cos(2k\tilde{t} + \varphi_h) \tag{2.23}$$

$$\alpha(t) = \alpha_a cos(2k\tilde{t} + \varphi_\alpha) \tag{2.24}$$

where $\tilde{t}$ is the dimensionless time and is equal to $\tilde{t} = \frac{t_{ref} U_{ref}}{L_{ref}}$.

Natural flyers generally use a combination of pitching and heaving motion rather than a single degree of freedom pitch or heave motion. With combined pitching and heaving motions the parameter space becomes larger, in addition to the pitch and heave amplitudes and oscillating frequencies, one now has to consider the phase angle between the pitch and heave motions. In figure 2.20, this situation is illustrated. Cases (a) and (b) represent the pure heave and pitch modes. In case (c) the airfoil is both pitching and heaving with a phase angle of 90 degrees (pure feathering). In case (d) and (e), the motion of case (c) is duplicated, but with a phase angle different that 90 degrees between the pitch and heave motions.

Above, we just presented the general $2\mathbb{D}$ case. For $3\mathbb{D}$ cases [9, 167], the scenario is far more complex as shown in figure 2.21. The wing-beat kinematics can be described by three positional angles within the stroke plane: (i) flapping about the x axis (rolling or flapping motion) in the wing-fixed coordinate system described by the positional angle ϕ, (ii) rotation of the wing about the z axis (lagging motion) described by the elevation angle θ, and (iii) rotation of the wing about the y axis (feathering motion) described by the angle of attack α. The angle of attack α is used to describe the orientation of a chordwise strip of a beating wing relative to the stroke plane, which may change significantly in the spanwise direction because of the wing torsion often observed in birds and insect flapping flight.

For a general $3\mathbb{D}$ case, definitions of the positional angle, the elevation angle, and the angle of attack, all in radians, are

$$\phi(t) = \sum_{n=0}^{3} \left[\phi_{cn} cos(2n\pi ft) + \phi_{sn} cos(2n\pi ft)\right], \quad n = integer \tag{2.25}$$

$$\theta(t) = \sum_{n=0}^{3} \left[\theta_{cn} cos(2n\pi ft) + \theta_{sn} cos(2n\pi ft)\right], \quad n = integer \tag{2.26}$$

$$\alpha(t) = \sum_{n=0}^{3} \left[\alpha_{cn} cos(2n\pi ft) + \alpha_{sn} cos(2n\pi ft)\right], \quad n = integer \tag{2.27}$$

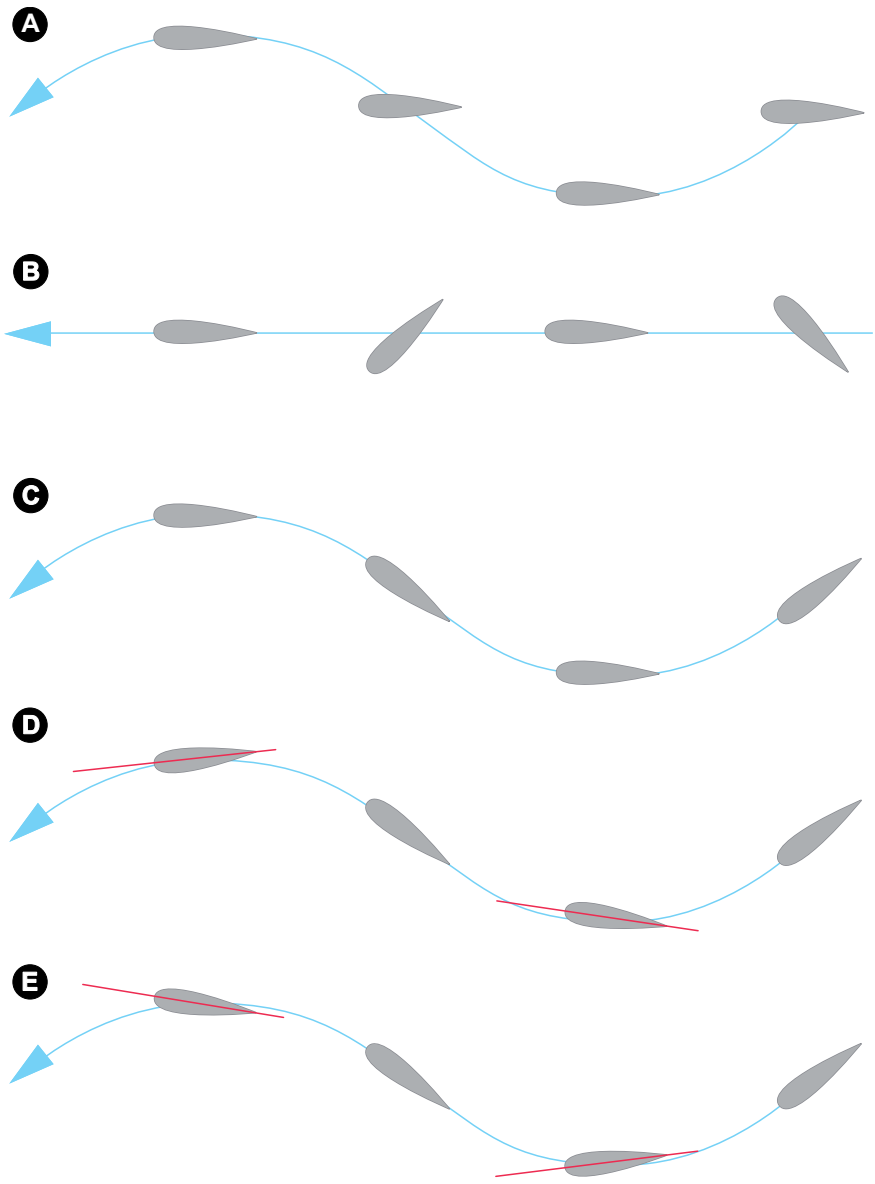

Figure 2.20: *Different possible combination of motions and effect of phase angle in* $2\mathbb{D}$.

Note that t is the time and f is the flapping frequency. The Fourier coefficients ϕ_{cn}, ϕ_{sn}, θ_{cn}, θ_{sn}, α_{cn} and α_{sn}, are determined from empirical kinematic data [114, 188, 213]. Based on the Fourier coefficients gathered by analysis of the kinematics of a hovering hawkmoth [114], the positional, elevation and feathering angle variation for one period are plotted in figure 2.22.

Equations 2.25, 2.26 and 2.27, represent the general $3\mathbb{D}$ case, where most if not all of the coefficients must be obtained from experimental data. However, simpler kinematics can be consider when dealing with $3\mathbb{D}$ cases, which are very similar or analogous to the kinematics in $2\mathbb{D}$ cases. Examples of such kinematics can be, a pure pitching wing, a pure heaving wing, a wing undergoing heaving-and-pitching motions, a wing undergoing lagging (or surging) and pitching motion

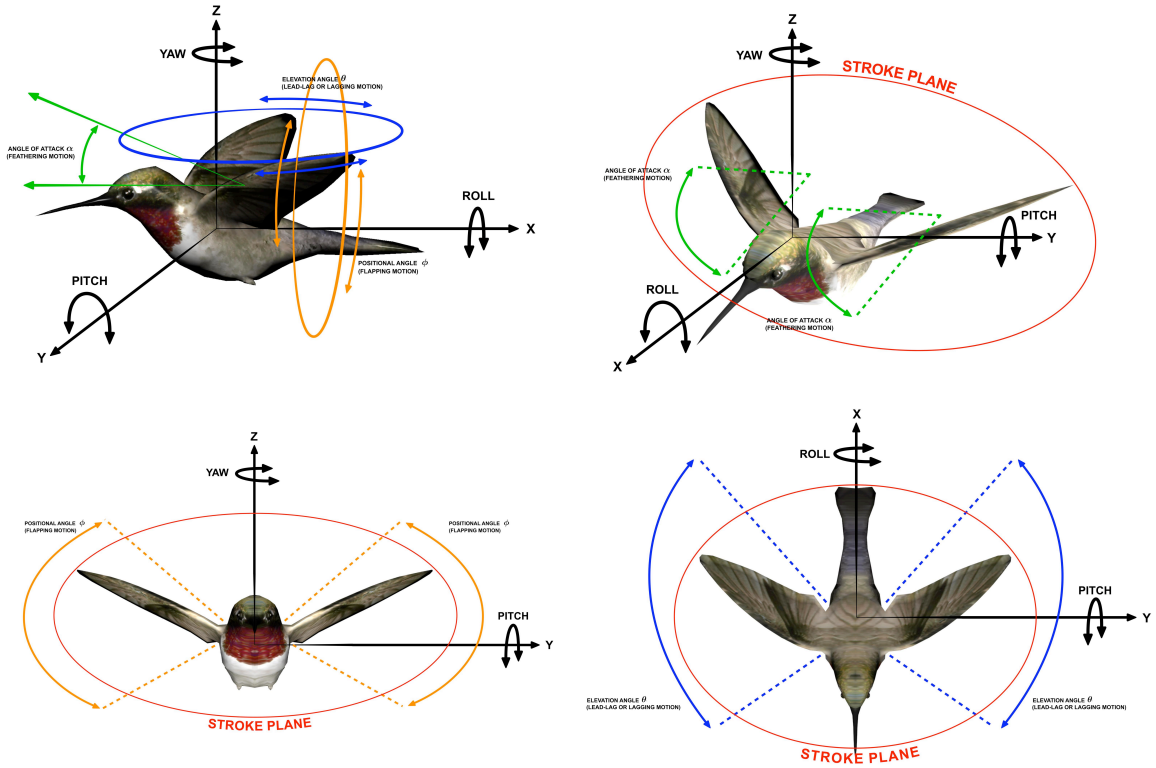

Figure 2.21: 3𝔻 *flapping wing kinematics.*

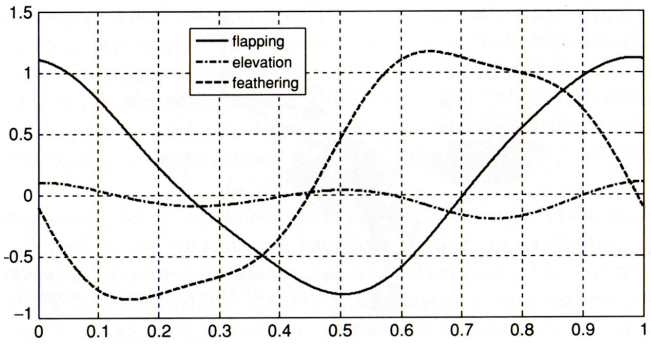

Figure 2.22: *Positional, elevation and feathering angle variations for one period for a hovering hawkmoth [167].*

or a wing rolling about the traveling axis, among others.

Even though 3𝔻 effects are important for predicting low Reynolds number flapping wing aerodynamics, 2𝔻 experiments and computations do provide important insight into the unsteady physics related to flapping wings, that is why a lot of research has been done and is being actively done in the field of 2𝔻 flapping airfoils aerodynamics [108, 140, 196, 198, 207, 216].